



Nonlinear dynamics of proton beams with hollow electron lens in the CERN high-luminosity LHC

D. Mirarchi^{1,2,a} , R. B. Appleby^{1,3}, R. Bruce², M. Giovannozzi², A. Mereghetti², S. Redaelli², G. Stancari⁴

¹ The University of Manchester, Manchester M13 9PL, UK

² CERN, European Organization for Nuclear Research, 1211 Geneva 23, Switzerland

³ The Cockcroft Institute, Warrington WA4 4AD, UK

⁴ Fermi National Accelerator Laboratory, Batavia, IL, USA

Received: 3 March 2021 / Accepted: 20 November 2021

© The Author(s) 2021

Abstract The design stored beam energy in the CERN high-luminosity large hadron collider (HL-LHC) upgrade is about 700 MJ, with about 36 MJ in the beam tails, according to estimates based on scaling considerations from measurements at the LHC. Such a large amount of stored energy in the beam tails poses serious challenges on its control and safe disposal. In particular, orbit jitters can cause significant losses on primary collimators, which can lead to accidental beam dumps, magnet quenches, or even permanent damage to collimators and other accelerator elements. Thus, active control of the diffusion speed of halo particles is necessary and the use of hollow electron lenses (HELs) represents the most promising approach to handle overpopulated tails at the HL-LHC. HEL is a very powerful and advanced tool that can be used for controlled depletion of beam tails, thus enhancing the performance of beam halo collimation. For these reasons, HELs have been recently included in the HL-LHC baseline. In this paper, we present detailed beam dynamics calculations performed with the goal of defining HEL specifications and operational scenarios for HL-LHC. The prospects for effective halo control in HL-LHC are presented.

1 Introduction

The current LHC collimation system [1–6] has achieved an excellent performance, delivering a halo-cleaning inefficiency of about 1×10^{-4} , which is defined as the loss leakage to sensitive equipment per impacting losses on the collimation system [7], thus ensuring safe operations without quenches from circulating beam losses with stored beam energies up to more than 300 MJ at 6.5 TeV [8]. Although this performance is very satisfactory and ensured the required operational flexibility, further improvements are necessary in view of the HL-LHC [9–13], whose design goal is to achieve stored beam energies of about 700 MJ at 7 TeV where also the power required to quench a magnet is lower. In this framework, the installation of HELs is now planned to improve various aspects of beam collimation and will take place during the Long Shutdown in 2025–2027.

Work supported by the HL-LHC project.

^a e-mail: daniele.mirarchi@cern.ch (corresponding author)

Table 1 Nominal HL-LHC beam parameters with colliding beams and standard filling pattern [17, 18], where σ is the transverse RMS beam size assuming a Gaussian proton beam distribution

Parameter	Value range
Beam energy [TeV]	7
Particles per bunch, N [10^{11}]	2.2
Maximum number of bunches per beam	2760
Stored energy [MJ]	681
Normalised transverse emittance ε^* [μm]	2.5
Stored energy above 3.6σ [MJ]	36
Desired 90% scraping time of particles above 3.6σ [min]	5
Tunes (Q_x, Q_y)	(62.31, 60.32)
Beam–beam tune shift/Interaction point (IP) ^a	0.01

^aMaximum total head-on tune shift of 0.02, as only two IPs will be colliding head-on

One of the main motivations comes from the requirement to handle the estimated stored energy present in the beam tails for all design loss scenarios. Various measurements carried out at the LHC indicate strong overpopulated tails with respect to a typical Gaussian transverse beam distribution [14–16]. Scaling these observations to HL-LHC beams, under the assumption that their population scales linearly with the bunch intensity, led to the conclusion that up to about 36 MJ might be stored in the beam tails [16]. The beam parameters of our interest are reported in Table 1, while a complete overview can be found in [17, 18]. Such a large amount of energy can cause unforeseen beam dumps, in case of orbit jitter, and fast-failure scenarios related for example to crab cavities (CC), due to the high beam losses that would take place on primary collimators [19, 20]. Moreover, the energy deposited during these events can lead to magnet quenches due to beam loss peaks around the machine, and in the worst case to permanent damages to collimators. Thus, a controlled and safe disposal of overpopulated beam tails has been recommended by three international review committees, carried out in recent years [21–23]. This can be achieved by a HEL, where the main proton beam travels inside a hollow electron beam over a few metres. The halo is affected by the electromagnetic field of the HEL, increasing its diffusion speed in a controlled manner. The halo is thus driven onto the collimation system and safely depleted. In 2019, HEL has been included in the HL-LHC upgrade baseline [13] as part of the collimation system, following the approval by CERN Council. Note that this new hardware will be built thanks to in-kind contributions from Russia and the United Kingdom.

Important milestones were achieved at Fermilab (FNAL) and Brookhaven (BNL). Two electron lenses generating a Gaussian electron beam were routinely used in operation at the Tevatron collider for long-range beam–beam compensation and abort gap cleaning [24–26]. Studies were also performed to characterise hollow electron beams as a function of magnetic field in the main solenoid and cathode–anode voltage [27], and to demonstrate halo scraping and reduced tail population with hollow electron beams [28, 29]. Two electron lenses are installed in the relativistic heavy ion collider (RHIC), which were used in proton–proton operations for head-on beam–beam compensation [30–37], generating a Gaussian electron beam also in this case. Currently, and until the completion of the sPHENIX detector upgrade, only heavy ions are used in operations at RHIC, which do not require head-on beam–beam compensation. Thus, the gun of the electron lens was changed in one ring in order to provide a hollow electron beam. Being the only active electron lens in the world, this provided a unique

opportunity to explore different operational scenarios for the HL-LHC through beam-based measurements in 2017–2018. Different beam tests have been performed and one of the main achievements was the successful demonstration that back-scattered electrons can be used to centre the electron beam around the circulating one. Moreover, measurements similar to those performed at Tevatron were repeated with 100 Z GeV Ru and 13.6 Z GeV Au beams, showing promising results not only in terms of halo removal, but also in terms of impact on the core, together with thorough investigations of hollow electron beam profile distortions and options to reduce them [38].

Preliminary tests at injection energy have been carried out at the LHC in 2016–2017 to study the effect of resonant dipole kicks, providing first useful insight into the effect of HEL residual fields acting on the beam core [39].

The main aim of the work in this paper is to provide precise simulations to support complex nonlinear beam dynamics considerations and HEL design choices. Of course, the HL-LHC operational cycle and optics are still evolving. Thus, considerations on expected beam dynamics with HEL in HL-LHC are also meant to provide a guideline on key studies that will be instrumental to finalise operational scenarios once the machine cycle and optics will be frozen.

An overview of main roles and concepts of beam collimation and HEL at HL-LHC is given in Sect. 2, while simulation tools used are introduced in Sect. 3. Frequency Map Analysis (FMA), studies of Dynamic Aperture (DA), halo depletion, and effects on beam core are reported in Sects. 4, 5, 6, and 7, respectively. Further considerations towards the definition of operational scenarios in HL-LHC are discussed in Sect. 8, while some conclusions are drawn in Sect. 9.

2 Beam collimation and HEL at the HL-LHC

The LHC demands a tight control of beam losses because of its cryogenic nature. Tens of mJ/cm^3 deposited in superconducting magnet coils by hadronic showers developed from circulating protons that are lost on them, can cause an abrupt loss of their superconducting properties, known as a magnet quench. On the other hand, more than 300 MJ were stored in the LHC circulating beams during Run 2, which will increase to about 700 MJ in HL-LHC. Thus, a highly efficient collimation system is mandatory to minimise the amount of deposited energy in the superconducting magnets by beam losses and hence avoid the risk of quenches that can lead to potential damage of ring hardware or reduction of the operation efficiency due to the recovery from quenches or beam dumps.

An illustrative picture of the working principle of the LHC collimation system is given in Fig. 1a. The current system [1–6] is composed of 44 movable ring collimators per beam, placed in a precise multi-stage hierarchy of gaps that must be maintained in any machine configuration to ensure optimal cleaning performance. Two LHC insertion regions (IRs) are dedicated to beam halo collimation: IR3 for momentum cleaning, i.e. removal of particles with a large energy offset, and IR7 for betatron cleaning, i.e. controlled disposal of transverse halo particles. Each collimation insertion features a hierarchy based on primary collimators (abbreviated TCPs), secondary collimators (TCSGs), and absorbers (TCLAs). In this scheme, the energy carried by the beam halo and intercepted by TCPs is distributed over several collimators (i.e. 19 collimators are installed in the betatron cleaning insertion per beam). Dedicated collimators for protection of sensitive equipment, e.g. the inner triplets in the experimental IRs, absorption of physics debris, and beam injection/dump protection are also present at specific locations of the ring. All collimators consist of two movable blocks

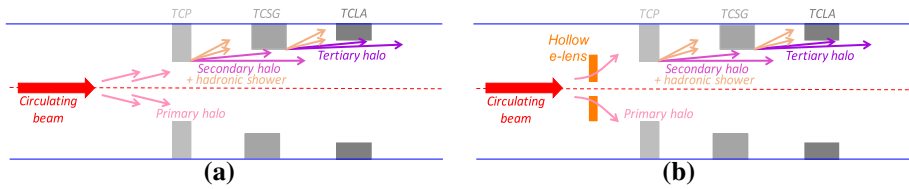


Fig. 1 Working principle of the **a** standard and **b** HEL-assisted collimation system in IR7

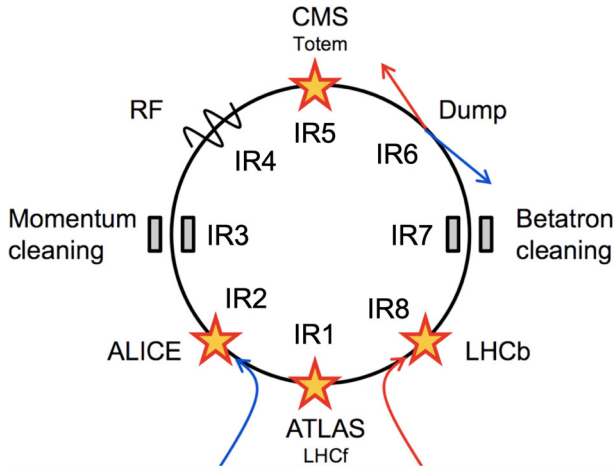


Fig. 2 Schematic layout of the LHC, where two HELs are planned to be installed in IR4 (one in each beam)

(except the single-sided dump protection block), called jaws. The jaws are centred around the circulating beam, with a well-established commissioning technique [5] that ensures optimum system performance. A detailed description of these functionalities goes beyond the scope of this paper and can be found in [1]. A schematic layout of the LHC is reported in Fig. 2: two counter-rotating beams are injected in IR2 and IR8 (in blue and red, respectively), the four main detectors ATLAS/ALICE/CMS/LHCb are housed in IR1/IR2/IR5/IR8, while the Radiofrequency (RF) cavities and extraction towards the beam dump are located in IR4 and IR6, respectively. Two HELs are planned to be installed in IR4 (one in each beam).

The main upgrades of the LHC collimation system that are part of the present HL-LHC baseline [10] involve the replacement of one Nb–Ti, 8.3 T dipole in the IR7 Dispersion Suppressor with two Nb₃Sn, 11 T dipoles with a collimator in between them, together with the replacement of some present collimators with new devices with jaws made of low-impedance material. Their aim is to improve the cleaning performance of the overall system, while reducing its contribution to the resistive-wall impedance budget of the ring. However, these upgrades do not allow for an active control on overpopulated beam tails and their safe disposal, for which the introduction of a HEL is deemed necessary.

2.1 HEL for HL-LHC

The HEL is a quite complex device, featuring a high-current electron source, up to 5 T superconducting solenoid magnets to guide and confine the electron beam, and a collector to dispose of the electron beam after its interaction with the proton beam. Tilted solenoids located

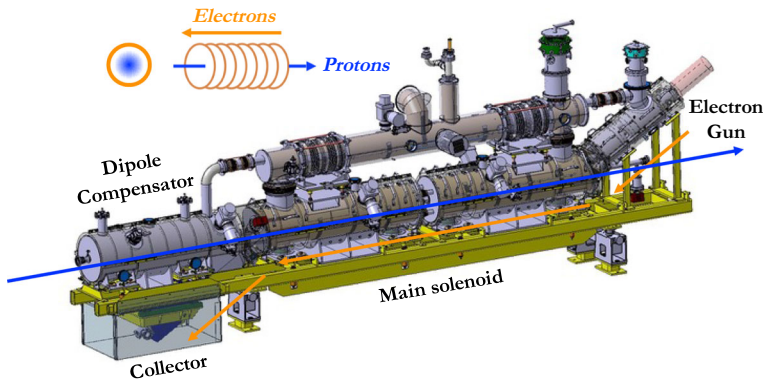


Fig. 3 Design of the HEL for HL-LHC [40]

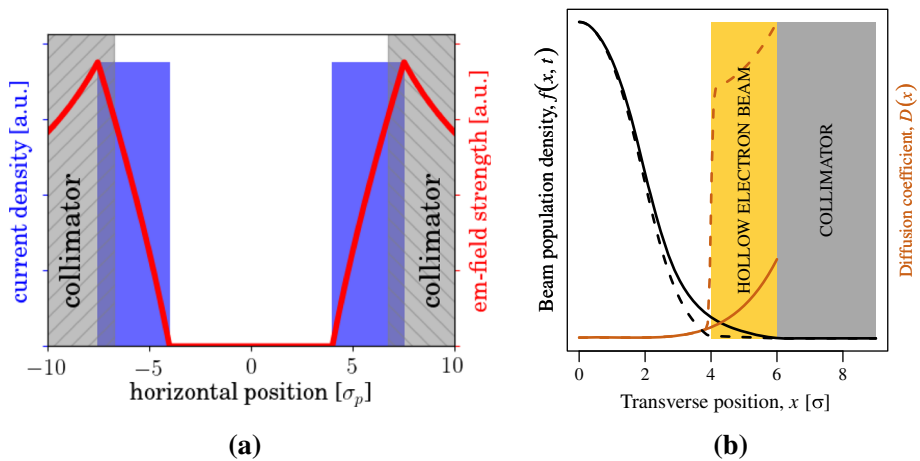


Fig. 4 **a** Schematic illustration of electromagnetic field generated by HEL [39] and **b** of halo population and diffusion coefficient with and without HEL shown by dashed and solid lines, respectively [39]

at both sides of the main ones are used to steer the electron beam on, and out, of the proton beam. The present design of the HEL for the HL-LHC is given in Fig. 3. Integration studies were performed, and candidate locations for the installation of HELs were identified at both sides of the IR4, based on technical considerations including the availability of a cryogenic system [40] and the increased separation between the two counter-rotating beams in this section. Beam-instrumentation concepts are based on the experience gathered at FNAL and BNL. In addition, a special gas jet curtain monitor will be added, to measure simultaneously the profile of the overlapping proton and electron beams [41, 42]. The main solenoid is split in two segments to enable the integration of this monitor in the centre of the HEL. The angular alignment between the two beams will be achieved with dedicated electron beam correctors, tuned using strip-line beam position monitor (BPMs) placed at the extremities of the main solenoid. A complete description of the magnetic design and beam instrumentation is out of the scope of this work and can be found in [40].

Note that several operational aspects were taken into account in the HEL design. A round pipe of 60 mm radius is foreseen, in order to avoid issues in terms of available aperture for

the circulating beam. The linear coupling stemming from the solenoidal fields was studied and showed to have a negligible effect on the circulating beam dynamics [43]. Impedance calculations of the full structure were performed, showing a negligible impact on the total ring-impedance budget [43], whereas effects of the electron beam on the dynamics of the circulating protons are the main focus of our studies.

The HEL is s-shaped in order to self-compensate edge effects generated by the in-coming and out-going electron beam on the proton beam core. However, the in-coming and out-going electron beam might not be identical leading to only a partial compensation, thus inducing a dipolar kick on the beam core. A disadvantage of this design is that the transverse components of the magnetic fields in the two steering solenoids add up and result in a net vertical kick experienced by the proton beam. This requires a dipole compensator (visible on the left side of Fig. 3) that compensates this net kick.

The symmetry of the electron distribution is crucial as dipolar and higher-order residual fields experienced by the proton beam must be minimised, because they can induce a nonzero dipolar or higher-order kick on the beam core. All these effects, except the dipolar kick from the bending solenoids, are negligible if the electron beam is powered at the same current at every turn, i.e. a DC mode is selected. However, they might become significant whenever it is envisaged to switch on and off the electron beam with specific pulsing pattern. Thus, extensive beam dynamics studies have been performed to determine the best compromise between operational needs and hardware feasibility, with the goal of defining operational scenarios that provide an optimal removal rate of beam tails throughout the cycle without jeopardising machine performance or protection.

An illustrative picture of the working principle of the HEL-assisted collimation is given in Fig. 1b. The present collimation system remains fully in place and the HEL is introduced as an additional hierarchy level. The active control of the primary-halo diffusion speed is achieved by overlapping the hollow electron beam and the circulating proton beam over a few metres, where the two beams travel in opposite direction to enhance the HEL performance [39]. This generates an electromagnetic field ideally acting only on particles with a transverse amplitude that is larger than the electron beam inner radius (r_1), as depicted in Fig. 4a, resulting in an increased diffusion speed that generates a depleted halo population, as schematically shown in Fig. 4b. Thus, for the purpose of the studies reported in this paper, let us assume as beam halo the fraction of circulating beam above r_1 , while the beam core is represented by the portion of circulating beam surrounded by the electron beam. The HEL performance is defined by the combination of halo removed and side effects on the beam core, i.e. the larger the fraction of halo removed without inducing a beam-core blow-up, the better the HEL performance.

Additional benefits from a controlled diffusion speed would be a possible increase in the impact parameters on TCPs, with an overall improvement of cleaning performance. If the impedance budget of the machine allows, collimator jaws could be closed at a smaller transverse amplitude thanks to the depleted halo, thus allowing a β^* and crossing-angle reduction for the high-luminosity experiments [44] located in IR1 (ATLAS) and IR5 (CMS).

2.2 Main HEL constraints and requirements

The detection of potentially dangerous losses using beam loss monitors (BLM) [45] is one of the most important observables for machine-protection purposes. A depleted halo could jeopardise the performance of the current machine-protection strategy. In fact, if beam tails are totally depleted and a beam instability develops, losses will become visible only when the beam core is approaching the primary collimators, which is a very dangerous situation. A solution could be based on the presence of trains of witness bunches, i.e. bunches on which

Table 2 Required functionalities of the HEL in HL-LHC (σ is the RMS beam size), assuming a Gaussian proton beam distribution and normalised emittance $\varepsilon^* = 2.5 \mu\text{m}$

Parameter	Value range
<i>Geometry</i>	
Length of the interaction region [m]	3
Minimum transverse scraping aperture (σ)	3.6
Minimum inner electron beam radius at 7 TeV [mm]	1.1
Inner vacuum chamber diameter [mm]	60
<i>Magnetic fields at 7 TeV and magnet parameters</i>	
Main solenoid field, B_m [T]	5.0
Gun solenoid field, B_g [T]	0.36–4.0
Bending solenoid field [T]	3.5
Compression factor, $\sqrt{B_m/B_g}$	3.8–1.1
Maximum current in main solenoid [A]	330
<i>Electron gun</i>	
Inner/outer cathode diameters [mm]	8.05–16.1
Peak yield at 10 kV [A]	5
<i>High-voltage modulator</i>	
Cathode–anode voltage [kV]	10–15 ^a
Rise time (10%–90%) [ns]	200
Pulse length [μs]	1.2–86

^a10 kV has been used for the work reported in this paper as conservative approach

the HEL does not act, combined with an appropriate relative scaling of allowed losses before triggering a beam dump. In addition, the HEL must not act on any particles in the abort gap, i.e. the range of the ring circumference left empty and synchronised with the rise-time of the dump kickers. In order to fulfil these constraints, the electron beam must be pulsed with a pattern satisfying the following characteristics:

- Rise and fall time of 200 ns, so that the HEL can be switched on or off in between different bunch trains, with the given train structure from the injectors.
- Pulse length ranging from 1.2 μs to 86 μs , in order to be active on a single train of 48 bunches with 25 ns spacing, up to the full beam except for the abort gap.¹

A complete list of HEL specification is reported in Table 2.

The main requirements on halo depletion are defined by fast-failure scenarios. The most dangerous events are related to CCs phase slip that can induce a longitudinal bunch rotation of up to 2σ [19,20,46], where σ is the RMS beam size, assuming a Gaussian beam distribution and normalised emittance $\varepsilon^* = 2.5 \mu\text{m}$. Thus, the HEL should be kept always on when CCs are on and must provide a depleted range of transverse amplitude of 2σ inside TCP aperture. On the other hand, the most dangerous events before beams are brought into collision are given by orbit jitter. They cannot be predicted and were relatively frequent during the Run 1 of the LHC (2009–2013) [47]. Thus, more aggressive halo removal strategies should be envisaged when the tail population reaches a dangerous level before collapsing the separation bumps. Quantitative considerations on the dangerous level of beam tails population are reported in [40], together with specifications on the amount and speed of tail depletion.

¹ One LHC turn is $\approx 89 \mu\text{s}$, and the abort gap length is 3 μs .

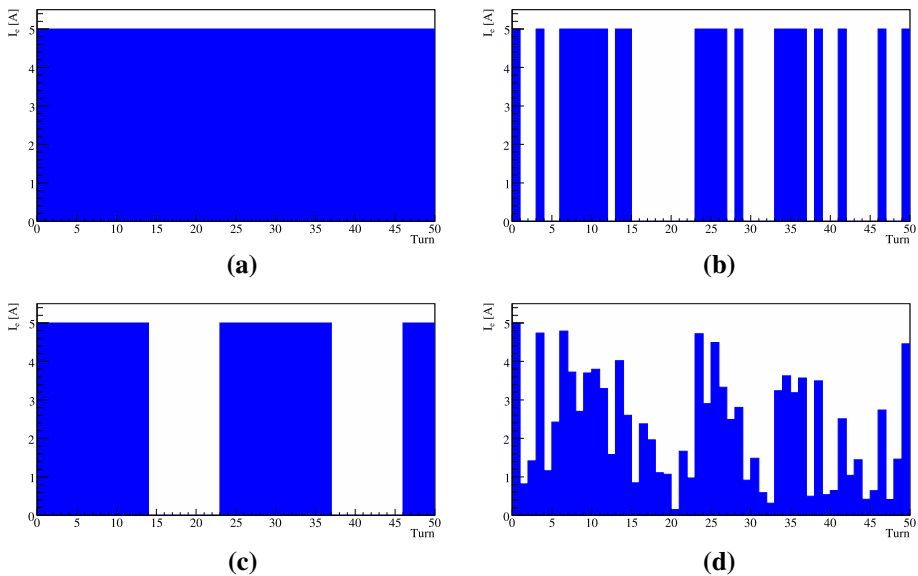


Fig. 5 Examples of HEL pulsing pattern: **a** DC, **b** $R_{0,5}$, **c** P_9^{14} , **d** R_I . The displayed values refer to current of the HEL during the passage of a bunch train that should be depleted, while it will be always off during the abort gap and the passage of witness trains

2.3 HEL pulsing pattern and machine configuration

The electron beam can be switched on and off with different patterns on a turn-by-turn basis determining the effect on both core and tails of the beam distribution. Possible modulation structures for the affected bunch trains (leaving out the abort gap and potentially witness trains as mentioned in Sect. 2.2) that have been studied are:

- *Continuous* (DC): the electron beam is always on at every turn.
- *Pulsed* (P_i^j): the electron beam is switched on for i turns and then off for j turns.
- *Random* (R_p): the electron beam is randomly switched on at each turn with a probability $p \in (0, 1)$.
- *Random current* (R_I): the electron beam is always on at every turn, but the current is randomly changed on a turn-by-turn basis according to a uniform distribution of values between 0 and 5 A.

Examples showing the excitation profile in time for the different schemes are reported in Fig. 5. Note the pulsed pattern R_I is the most challenging from the hardware point of view, and, although other patterns featuring changes of electron beam current could be envisaged, one of the main scopes of these studies is to identify the best compromise between required HEL performance and hardware feasibility.

The main machine parameters used for all the studies reported in this paper are listed in Table 3. The HL-LHC will be operated with levelled luminosity, which is achieved by means of a dynamic β^* squeeze while beams are colliding [9–13]. On the other hand, the machine configuration presently available for our purposes features the smallest β^* , corresponding to the last luminosity levelling step. Furthermore, it is worth stressing that this optical configuration has been used in combination with the IR bumps that keep the beams separated at the interaction points and without taking into account any long-range beam–beam effects.

Table 3 Main machine parameters

Parameter	Value
Beam energy [TeV]	7
Optics version	HL-LHCv1.3
β^* Interaction Point (IP) 1/2/5/8 [m]	0.15/10/0.15/3
ε^* [μm]	2.5
Half crossing angle IP 1/2/5/8 [μrad]	250/170/250/ – 250
Half parallel separation IP 1/2/5/8 [mm]	–0.75/2/0.75/ – 2
Tunes (Q_x, Q_y)	(62.31, 60.32)
Chromaticity (Q')	15
Landau octupole current (I_{MO}) [A]	–300
Linear coupling ($ C^- $)	0

However, this is not expected to have a major impact on the results reported in this paper because strong nonlinearities are present in the lattice used, which are the main driving term of HEL performance. Effects from nonlinearities due to field imperfections in the inner triplet may vary as a function of β^* , but are expected to be negligible given the overall field quality. On the other hand, the tune footprint is significantly affected by head-on beam–beam and it would be certainly interesting to repeat the studies reported here for a more detailed evaluation of expected HEL performance with colliding beams.

3 Simulation tools

The studies reported in this paper were carried out using `SixTrack` [48–52] that allows a symplectic, fully chromatic, and 6D tracking along the magnetic lattice of the machine, taking into account interactions with the ring collimators and the detailed aperture model of the entire ring. `SixTrack` has been successfully benchmarked with data of LHC beam loss patterns in [3, 53–58].

Frequency map analysis (FMA) and dynamic aperture (DA) simulations are relatively faster than full halo-depletion simulations. In particular, simulations to compute FMAs require few hours, several hours are needed for DA simulations, and few days for complete halo-depletion studies, running on the CERN Batch Service or on the BOINC platform for distributed computing [59–61]. Thus, FMA and DA studies were performed to explore the available parameter space and to guide the choice of a subset of promising HEL configurations. Then, a detailed evaluation of the tail depletion rates and the impact on the beam core were performed for these selected subsets of cases only.

An ideal HEL was implemented in `SixTrack` and it was used for DA, FMA, and halo-depletion simulations. An electron beam with uniform radial distribution was considered, without taking into account edge effects from the electron beam injection and extraction stages. Thus, the radial kick experienced by the circulating protons can be modelled as:

$$\theta(r) = \begin{cases} 0 & \text{if } r < r_1, \\ \frac{r^2 - r_1^2}{r_2^2 - r_1^2} \frac{\theta_{r_2}}{r/r_2} & \text{if } r_1 < r < r_2, \\ \frac{\theta_{r_2}}{r/r_2} & \text{if } r > r_2 \end{cases} \quad (1)$$

where r_2 is the outer radius of the electron beam and θ_{r_2} is the maximum kick achieved at $r = r_2$, which can be expressed as:

$$\theta_{r_2} = \frac{1}{4\pi\epsilon_0} \frac{2I_e L (1 \pm \beta_e \beta_p)}{r_2 \beta_e \beta_p c^2 (B\rho)_p}, \quad (2)$$

where $v_e = \beta_e c$ is the electron velocity, $v_p = \beta_p c$ the proton velocity, and $(B\rho)_p$ is the magnetic rigidity of the proton beam. The '+' sign applies when the magnetic force is directed like the electrostatic attraction ($v_e \cdot v_p < 0$), whereas the '-' sign applies when $v_e \cdot v_p > 0$. For example, in the HL-LHC configuration with an electron beam current $I_e = 5$ A, an interaction region of length $L = 3$ m, $\beta_e = 0.237$ (corresponding to 15 keV electrons), $r_2 = 2.2$ mm, the corresponding maximum kick is $\theta_{r_2} = 0.3$ μ rad for 7-TeV protons anti-parallel to the electrons.

The treatment described above implies that the residual field acting on the beam core was disregarded. Thus, this ideal HEL implementation was replaced by a dipolar kick for studies of emittance growth as a first-order approximation. Note that a complete and general HEL description is by now available in `SixTrack`. It is based on Chebyshev polynomials [62] and makes it possible to take into account simultaneously the phenomena impacting on the tails and on the core. Note the approach used to generate the results presented in this paper is fully adequate for our purposes, and the new tools will be used for the definition of the final HEL operational scenarios, once the HL-LHC operational cycle will be frozen.

4 Frequency map analysis

FMA is a technique that has become standard in accelerator physics to study the behaviour of initial conditions and assess whether they generate chaotic or regular orbits. The roots of this approach are in the domain of celestial mechanics (see, e.g. [63] and references therein for an overview). The essence of the method is the fundamental property of chaotic orbits, namely that they do not belong to a regular torus and hence there is no well-defined frequency associated with the initial condition. This implies that whenever an estimate of the orbit frequencies ν_z with $z = x, y$ is performed by using two segments of an orbit, i.e. using the data between turn 1 and N and then between $N + M + 1$ and $2N + M$ with N, M integers, then the quantity $\Delta\nu(N) = \sqrt{(v_x(N) - v_x(2N))^2 + (v_y(N) - v_y(2N))^2}$, where $\nu_z(N)$ and $\nu_z(2N)$ represent the frequencies evaluated over the first part and the second part of the orbit, respectively, then $\Delta\nu(N)$ is bounded away from zero when $N \rightarrow \infty$ in the case of a chaotic orbit. In the applications, the limit is never evaluated, but it is assumed that if $\Delta\nu(N)$ is not small, then the orbit is chaotic. It is obvious that this criterion is rather qualitative, although it is possible to make it more quantitative and use it to detect chaoticity (see, e.g. [64,65] and references therein for an overview).

The main application of FMAs to our purpose is to identify driving terms that enhance halo diffusion speed, using simulations that are relatively fast as introduced in Sect. 3. Typical simulation parameters of LHC beam-beam studies were used, such as 10^5 simulated turns with the betatron tune evaluated in the first and last 3×10^3 turns. However, further studies are needed to adapt these parameters to the specific HEL pulse under study. This is because different pulses can have significantly different performances: while a low-efficiency pulse is still pushing particles towards resonance lines, a highly efficient pulse can make particles drift far away in the tune space in the same number of turns; thus making impossible to quantitatively estimate driving terms in both cases.

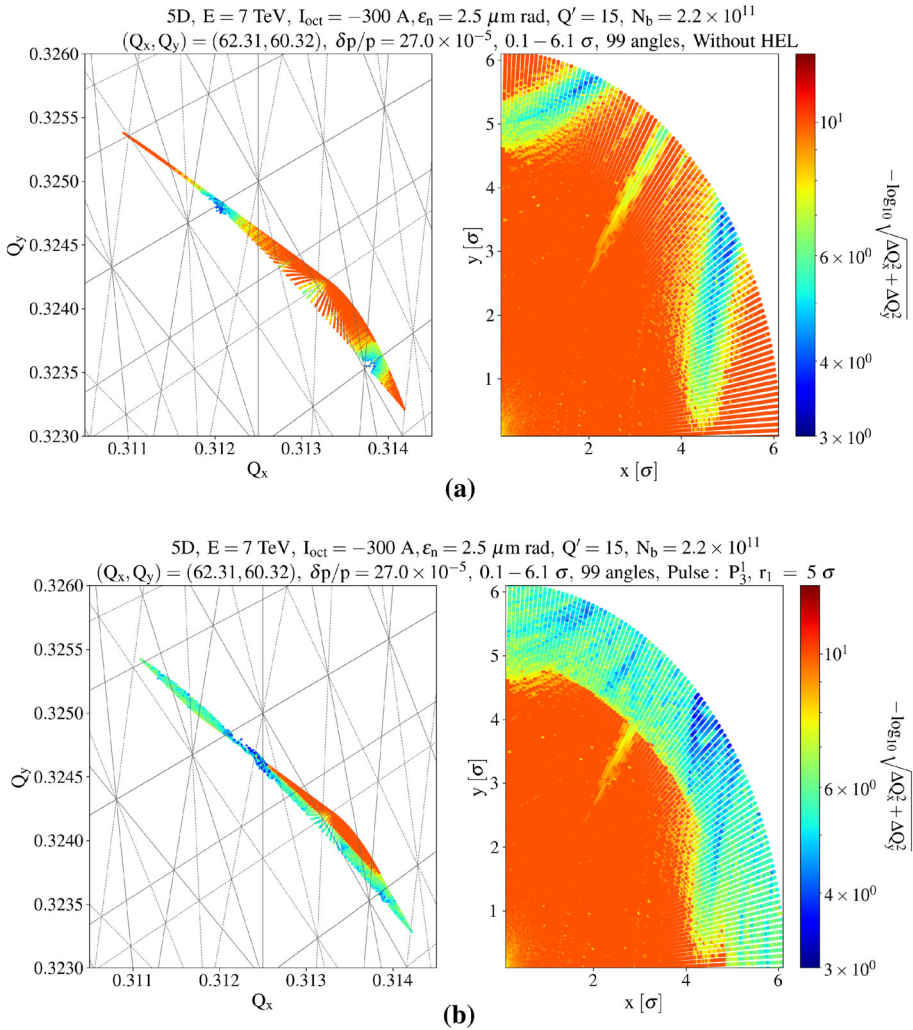


Fig. 6 Example for FMAs for **a** reference HL-LHC case without HEL and **b** with HEL with pulse P_3^1 and $r_1 = 5 \sigma$. Resonance lines up to 23rd order are shown in the tune footprint (left)

Nevertheless, a qualitative picture can be given as shown in Fig. 6, where regions of lower stability are highlighted by the blue areas. A uniform beam distribution is generated in the range $0.1 - 6.1 \sigma$ for 99 angles covering the $x - y$ plane. The synchrotron motion is not considered and all particles are generated with a momentum offset of $\delta p/p = 27 \times 10^{-5}$. The HEL effect is clearly visible comparing Fig. 6a and b. A quite sharp stability step is present in Fig. 6b (right) at 5σ , which is where the HEL r_1 is set. The tune footprint in Fig. 6b (left) shows a clear distortion, with the HEL providing a positive tune shift eventually leading to a folding. Another observation is that the HEL couples with machine nonlinearities, enhancing instabilities already present, as expected [66]. The main driving terms generating less stable regions in Fig. 6a (left), which are broadened by the HEL as shown in Fig. 6b (left), are due to 9th (bottom-right), 14th (top-left), and 16th (middle) order resonance lines.

Table 4 Main parameters used in the DA simulations

Parameter	Value
<i>HEL</i>	
Inner radius (r_1) [σ]	3–9 with step of 2
Pulse	DC, R_p , P_j^i , R_I
Electron beam current (I_e) [A]	1–5 with step of 1
<i>HL-LHC lattice</i>	
Q'	0, 2, 5, 10, 15
I_{MO} [A]	–600 to 300 with step of 150
<i>Tracking</i>	
Turns	10^6
x – y angles [deg]	0–90 with step of 5.3
Amplitudes [σ]	2–22 with step of 2
Seeds	60

5 Dynamic aperture studies

The DA represents the extent of the phase-space volume in which the particle motion remains bounded over a given number of turns (see [67–69] and references therein for an overview of this topic). Although its definition is rather abstract, this figure of merit is an essential one for evaluation of the impact of nonlinear beam dynamics on the performance of a circular particle accelerator. Indeed, it is possible to establish a link between the evolution in the time of the DA and the corresponding variation of beam intensity [70] and luminosity evolution [71, 72], which clarifies the relevance of DA for accelerator physics.

As far as the ring description is concerned, the measured magnetic errors for the LHC have been included in the simulations as well as the expected errors for the future HL-LHC magnets. It is worth mentioning that sixty different realisations (also called seeds in the following) of the magnetic field errors are considered in the computation of the DA. The reason for this is twofold: firstly, not all the LHC magnets have been measured in cold conditions. For the cases in which the field quality had been measured at warm conditions, only, the warm-to-cold correlations had to be applied, and these quantities are affected by an uncertainty that is probed by the various realisations. Secondly, the magnetic field errors for the new HL-LHC magnets are known only by means of electromagnetic simulations, which take into account the possible impact of the mechanical tolerances of the coils' geometry. Hence, the field quality is known as a series of multipolar coefficients with a certain statistical distribution.

The different parameters for the HEL settings and machine nonlinearities used, and those that were probed in the DA simulations are reported in Table 4. Note that the typical results of DA simulations can be shown as:

- Average DA over all seeds as a function of $x - y$ angle, with envelope given by absolute minimum and maximum DA over all seeds.
- Average DA over all seeds and angles, with error bars given by the absolute minimum and maximum DA over all seeds and angles.

Qualitatively, the closer the DA is to r_1 , the more efficient the excitation mode. An example of results obtained when changing r_1 is given in Fig. 7, where $Q' = 2$ and $I_{MO} = 0$ A. The

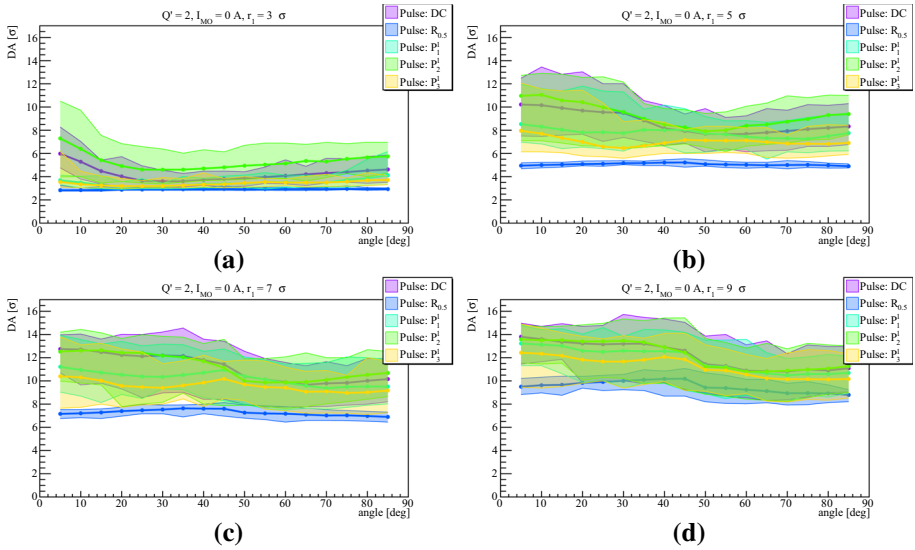


Fig. 7 Examples of DA for different HEL pulses and inner radius of **a** $r_1 = 3\sigma$, **b** $r_1 = 5\sigma$, **c** $r_1 = 7\sigma$, **d** $r_1 = 9\sigma$, with $Q' = 2$ and $I_{MO} = 0$ A

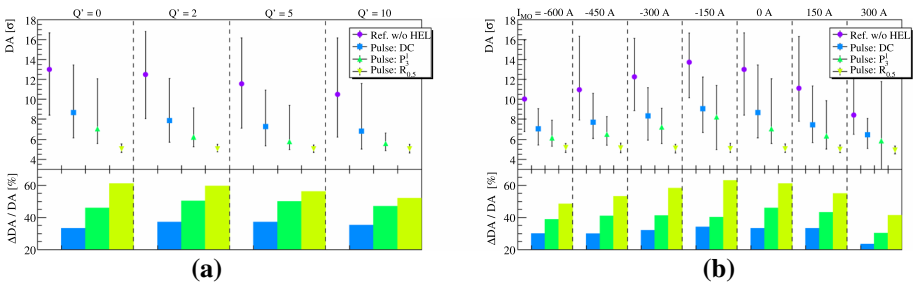


Fig. 8 **a** Effect of Q' on DA for different HEL pulses (with $I_{MO} = 0$ A and $r_1 = 5\sigma$), **b** effect of I_{MO} on DA for different HEL pulses (with $Q' = 2$ and $r_1 = 5\sigma$)

latter condition is used to probe the genuine impact of the HEL on the beam dynamics without the combined effect of the strong octupoles used in operations to stabilise the beams. The pulse pattern $R_{0.5}$ is the most efficient and sets the average DA almost exactly at r_1 for all angles, with a spread that increases linearly as a function of r_1 . The other pulses (DC, P_1^1 , P_2^1 , P_3^1) are found to be much less efficient, given the relatively larger DA obtained. It is interesting to note that the larger r_1 the smaller is the difference of DA for the various pulse patterns. This observation can be explained by the fact that nonlinear beam dynamics is dominated at larger amplitudes by the magnetic field errors, rather than the HEL, as the electron beam density decreases with increasing phase-space amplitude,² thus leading to smaller kicks. These two factors level out the performance of the different patterns when increasing r_1 .

The results obtained probing the effects of the HEL on DA with different settings of Q' and I_{MO} are shown in Fig. 8a, b, respectively. The pulse $R_{0.5}$ is always the most efficient and sets the average DA almost exactly at r_1 , regardless of the value of Q' or I_{MO} . For the other

² The outer radius (r_2), given by magnetic compression, is $r_2 = 2r_1$, see Table 2.

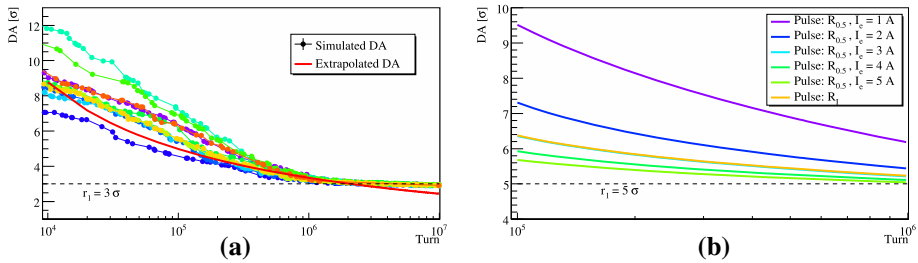


Fig. 9 **a** Several simulated seeds and extrapolated DA evolution for pulse P_3^1 with $Q' = 2$, $I_{MO} = 0$ A, and $r_1 = 3\sigma$. **b** Average DA evolution for pulse $R_{0,5}$ and different electron beam current and for pulse R_1 , with $Q' = 2$, $I_{MO} = 0$ A, and $r_1 = 5\sigma$

pulse types, larger values of Q' are beneficial for HEL performance, i.e. facilitate in lowering the DA closer to r_1 . However, it is the reference DA without HEL that decreases by itself as a function of Q' and the relative DA reduction obtained by using HEL is quite consistent for all cases. Moving to the I_{MO} scan, the trend of DA variation is almost symmetric with respect to $I_{MO} = -150$ A, which features the largest reference DA. Positive I_{MO} might be beneficial for HEL performance, i.e. less octupole current is needed to achieve the same DA (DA at $I_{MO} = -450$ A \equiv DA at $I_{MO} = 150$ A). Note also that other constraints, mainly due to beam stability considerations, determine the choice of the HL-LHC baseline values that are $Q' = 15(20)$ and $I_{MO} = -235(-40)$ A at 7 TeV (450 GeV) [17], which means that the chromaticity and octupole strength are not free parameters for the optimisation of the HEL performance. The relative DA reduction obtained with the HEL is quite stable also as a function of I_{MO} , except with $I_{MO} = 300$ A for which a relatively small reference DA is present.

Other useful information on the expected HEL performance can be provided by the behaviour of DA as a function of the simulated number of turns. In particular, the faster the DA approaches r_1 , the more efficient is the pulse pattern under study. Parametric fits can be used to extrapolate the DA to much larger turn numbers without the need of performing complete tracking simulations. Two models were used to describe the DA evolution [73], which were developed taking into account diffusive mechanisms that are linked to nonlinear beam dynamics in particle accelerators. In this respect, the HEL provides an additional diffusive term that can be included in the framework that was used in [73] to derive the DA models. However, it should be stressed that the effect of the HEL is not continuous as a function of amplitude, like any other transverse nonlinear effect, as below r_1 the HEL is not affecting the beam dynamics any longer. Parametric studies were performed to define the minimum value of the turn number for the fit convergence. The average DA evolution over 60 seeds was evaluated and the agreement between the two models in [73] was checked, showing differences below 4% over 10^9 turns (about 24 h LHC beam time). An interesting feature was observed in some extrapolated DA that were becoming smaller than r_1 . Thus, checks were performed using the pulse P_3^1 with $Q' = 2$, $I_{MO} = 0$ A, and $r_1 = 3\sigma$, which showed an extrapolated DA smaller than r_1 . The comparison between several simulated seeds and extrapolated DA is reported in Fig. 9a, showing that, as expected, $DA < r_1$ are an artefact of the extrapolation because of the non-continuous dependence of the HEL kick on the amplitude. Thus, the turn number at which extrapolated DA crosses r_1 should be considered as stabilisation point of DA at r_1 . This is a very important piece of information, because it provides a first quantitative estimation of the time needed to completely deplete the primary beam halo by a given HEL

pulse pattern, which is achieved when the DA reaches r_1 , as further discussed in Sect. 6. In conclusion, DA evolution models [73] describe well the extrapolated average behaviour and can be very useful to give indications on the relative efficiency of HEL pulse types without the need of extremely long and CPU-intensive numerical simulations. In particular, the smaller the initial DA and the time needed to approach r_1 , the more efficient the HEL pulse.

Studies of the dependence on Q' and I_{MO} were performed, leading to conclusions similar to what previously discussed. In particular, the pulse $R_{0.5}$ is always the most efficient and brings very quickly the DA almost exactly at r_1 regardless of the value of Q' or I_{MO} . For the other pulses, similar observations as in Fig. 8a, b can be made, e.g. the larger the Q' the smaller the initial DA and the faster the decrease towards r_1 .

DA evolution as a function of electron beam current (I_e) was also studied and an example is reported in Fig. 9b, where the pulses $R_{0.5}$ and R_I are compared. The smaller the I_e , the smaller the efficiency of the pulse $R_{0.5}$, as expected. On the other hand, the decrease in efficiency is not linear as a function of I_e , giving a first indication of potential margins of optimisation of the value of I_e . This is a very useful observation, because reducing the electron beam current without a significant loss of halo-depletion performance can have several advantages, as discussed in Sects. 6 and 7. Another important conclusion that can be extracted from Fig. 9b, is that the expected performance of the pulse R_I is comparable to $R_{0.5}$ with reduced $I_e = 3$ A. Given the hardware complexity to realise the pulse R_I , this observation provides a first indication that requirements on having this pulse type available for HL-LHC may be relaxed.

6 Halo-depletion studies

The DA represents the extent of the phase-space in which stable motion occurs. Thus, it may sound reasonable to estimate the fraction of beam halo removed by the HEL by means of DA simulations, only. However, considering all particles above the DA as lost can lead to an underestimation of the actual HEL performance, except if $DA = r_1$, as shown in Fig. 10. This is due to the fact that any estimate of the beam halo removal based on the knowledge of the DA has to assume that the beam distribution is time independent, whereas this assumption is violated in reality, and the violation increases the larger is the difference between the value of the DA and r_1 . Therefore, only if either the pulse pattern is very efficient or the DA simulations are carried out for a large enough number of turns, to achieve a situation in which $DA \approx r_1$, the DA is an effective figure of merit to assess the halo removal impact. Otherwise, complete halo-depletion simulations are needed for a quantitative evaluation of the expected HEL performance.

Only horizontal and vertical TCPs were taken into account in these simulations and were treated as perfect absorbers without accounting for the particle-matter interactions, which also means that the evaluated HEL efficiency is to be considered as an upper bound to the actual situation. This configuration has been chosen because there is no need to simulate the loss pattern along the entire machine at this stage (for which a realistic treatment of particle interaction with collimators is crucial) and allowed reducing significantly the CPU time needed.

Several configurations were probed using the parameters listed in Table 3, with primary collimators at 6.7σ as for the HL-LHC baseline [17]. The HEL inner radius was kept constant at $r_1 = 5\sigma$ in order to have results that can be compared with DA simulations reported in Sect. 5.

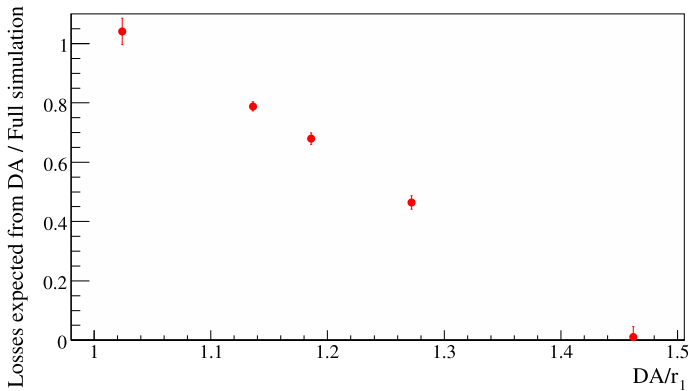


Fig. 10 Estimate of the expected beam halo removal using only the results of DA simulations normalised by the estimate obtained with full simulations, as a function of the ratio between DA and r_1

The results presented and discussed in this section must be combined with the expected impact on beam core, discussed in Sect. 7, in order to build a first proposal of an operational scenario for HL-LHC, which will be presented in Sect. 8. It is important to note that halo re-population mechanisms are not considered in these simulations, although they should be taken into account in future studies to provide refined predictions and an improved operational scenario. Note that a re-population time of several tens of seconds for tails above 5σ is expected, assuming a similar diffusion coefficient as that measured recently at the LHC [16].

6.1 Random excitation

A comparison between the computed performance with pulse $R_{0.5}$ for different electron beam current and pulse R_I is reported in Fig. 11. These results are in good qualitative agreement with those obtained from the evolution of DA over time, shown in Fig. 9b. More quantitatively, it is possible to observe that the pulse $R_{0.5}$ is very efficient and more than 50% of the particles above r_1 are expected to be removed after 10s of HEL excitation. The amount of halo particles removed is not linearly dependent on I_e , as indicated also by the DA studies. Significant margin is present on the available electron beam current, which can possibly be reduced at the expense of having $\sim 5\%$ to $\sim 10\%$ less halo particles removed after 10s, when going from 5 to 4 A or from 2 to 1 A, respectively. This observation could provide a very useful mitigation measure in case of limitations on current delivered by the electron gun, power deposition on the electron collector, and large residual field on the beam core. Another important observation, which is in agreement with the qualitative behaviour shown in Fig. 9b, is that the halo depletion with the pulse R_I is equivalent to the one obtained with $R_{0.5}$ and $I_e = 3$ A. This quantitative assessment shows that from the halo removal point of view there is no need to search for complex hardware solutions to make the pulse type R_I feasible.

A scan of probability p ranging from 5 to 95% in steps of 5% for the pulse R_p has been performed, while keeping the electron beam current at 5 A. A rather large plateau has been observed, which ensures stable performance for $35\% \leq p \leq 65\%$, as shown in Fig. 12. Performance is reduced for $p < 35\%$ or for $p > 65\%$, because either the HEL is acting, on average, for too few turns, or it is losing its randomness being on, on average, for too many turns, respectively. Therefore, $p < 35\%$ might represent a useful interval for p in the case

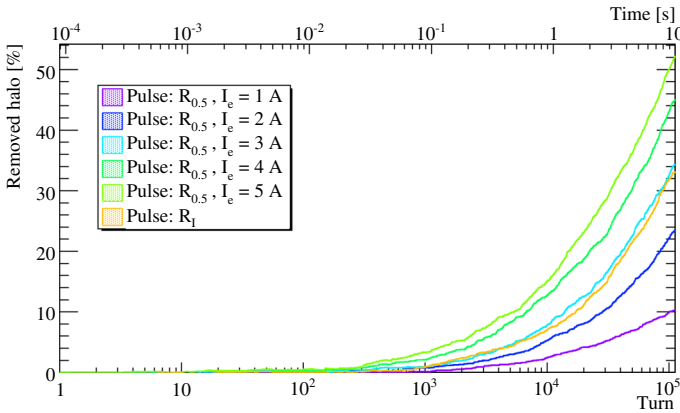


Fig. 11 Estimate of the expected beam halo removal as a function of time with pulse $R_{0.5}$ and different electron beam current, and with pulse R_I , with $r_1 = 5 \sigma$

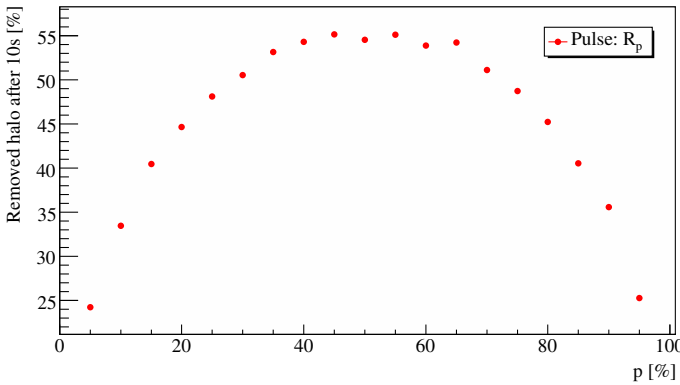


Fig. 12 Estimate of the expected beam halo removal after 10 s for different probability values p ranging from 5 to 95% in steps of 5% for the pulse type R_p , with $r_1 = 5 \sigma$

of limitations on power deposition on the electron collector, and of large residual fields on the beam core, while still providing a significant halo depletion.

In conclusion, the pulse R_p is very efficient thanks to its spectral content (white noise). This means that resonant kicks are given to all particles above r_1 , enhancing their diffusion speed towards primary collimators.

Excitation pulses tuned on the frequency content of the beam halo were also studied. Unfortunately, the main drawback is that they would not be easy to implement operationally. Moreover, an excitation window tuned around the halo frequency content will induce a relatively fast halo diffusion initially, which vanishes as soon as particles drift outside the excitation window. Thus, the frequency interval to be covered by the HEL excitation should be such to cover the typical frequencies of particles with amplitude ranging from r_1 up to the primary-collimator aperture.

In both cases of white noise (R_p) and tuned noise, resonant kicks will be given also to the beam core. This is because white noise includes those frequencies by definition and the excitation window of tuned noise will range around betatronic tunes of the beam core, as

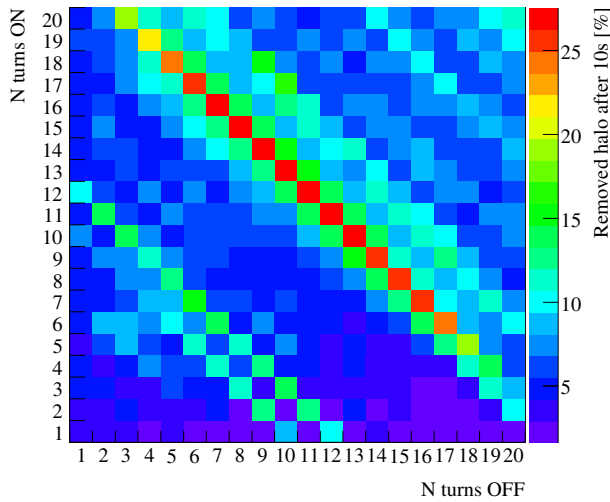


Fig. 13 Estimate of the expected beam halo removal after 10 s for different combinations of P_j^i

qualitatively visible in Fig. 6b. This implies that the core will be significantly affected by residual fields, as discussed in detail in Sect. 7.

6.2 Deterministic excitation

Switching on the electron beam for one turn and then off for n turns (i.e. P_n^1) had always been considered for deterministic excitation in previous studies [39]. In this work, this type of pulsing scheme was generalised by varying both parameters, i.e. the number of turns for which the pulse is on or off, thus creating a 2D function. Figure 13 shows the beam halo removal as a function of the two parameters of the pulse type. Some structure is clearly visible. The highest beam halo removal is achieved for a period of $T = 23$ turns, obtained for the machine parameters listed in Table 3, with P_9^{14} showing the best performance, with about 28% of beam tails removed after 10 s. Investigations were performed to probe larger T while moving along the path $T = P_1^1, P_2^1, P_2^2, P_3^2, \dots, P_{50}^{50}$, thus until $T = 100$. The pulse pattern P_9^{14} is the most efficient over this extended scan range.

The impact of chromaticity and Landau octupoles was probed too. While almost no changes are observed when varying Q' , the best value of T depends on I_{MO} , as shown in Fig. 14.

Ongoing work is expected to build on these results to shed some light on the features observed in the dependence of the beam halo removal on the shape of the deterministic pulse.

6.3 Continuous excitation

The DC pulse is expected to be that with the smallest impact on the beam core, because it generates a constant kick in time due to residual field, even though it is also the least efficient in terms of beam halo depletion, exactly for the same reason. A comparison between expected beam halo removal after 100 s induced by the pulses $R_{0,5}$, P_9^{14} , DC, is shown in Fig. 15.

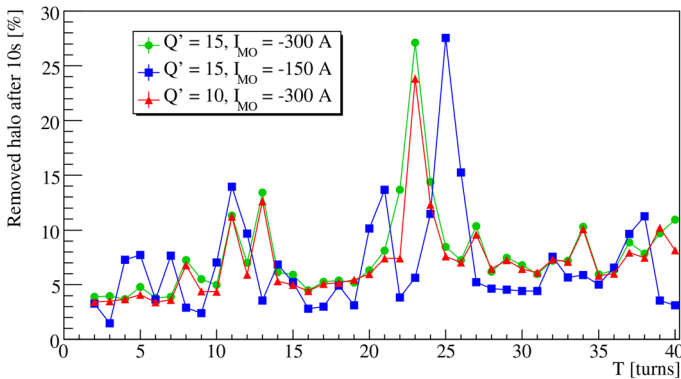


Fig. 14 Estimate of the expected beam halo removal after 10s as a function of T and for different values of Q' and I_{MO}

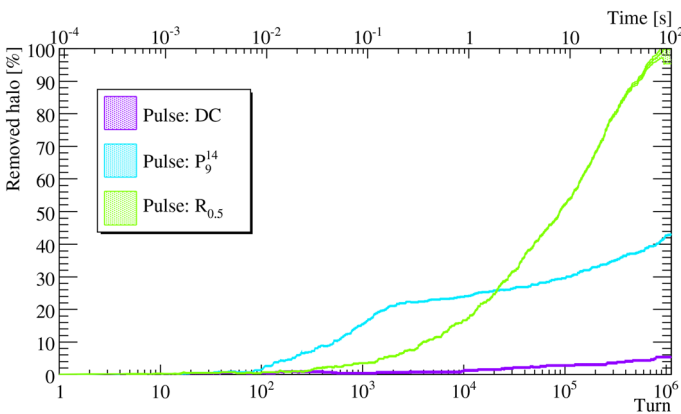


Fig. 15 Estimate of the expected beam halo removal after 100 s for various HEL pulsing patterns

The difference in efficiency of the three types of pulses is clearly visible. The HEL performance is enhanced by nonlinearities [66] in the machine and the DC is expected to be more efficient when tacking into account also beam–beam effects, which are out of the scope of this work and should be considered when defining the final operational scenarios in HL-LHC.

7 Impact on beam core and its mitigation

Core blow-up induced by the HEL must be avoided because it jeopardises machine performance, such as luminosity reach. The ideal HEL implementation used in Sect. 6 was replaced with a vertical dipolar kick to carry out the studies on the potential emittance growth of the core. Such a vertical kick is dynamically tuned accordingly to the pulse pattern under investigation. The estimated residual kick with the current HL-LHC HEL design is about 5 nrad and below 0.1 nrad in the vertical and horizontal planes, respectively [74]. Hence, only the vertical residual kick was simulated, being the dominant contribution as shown below. Note that the acceptable continuous emittance blow-up in HL-LHC is below $0.05 \mu\text{m/h}$ [17].

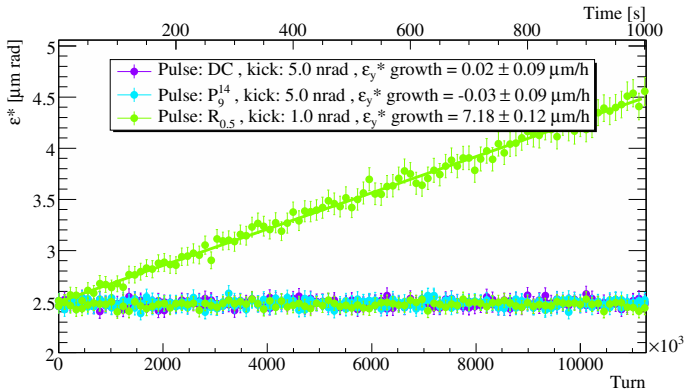


Fig. 16 Emittance evolution for different HEL pulse patterns. Solid and dashed lines represent the expected trend in the vertical and horizontal planes, respectively

Several cases were studied with the number of simulated turns reaching up to 10^7 to be as close as possible to the requested sensitivity of $0.05 \mu\text{m}/\text{h}$. The results are shown in Fig. 16, where solid and dashed lines represent the expected trend in the vertical and horizontal planes, respectively. An emittance growth within the acceptable limit is found for the pulses DC and P_9^{14} , as shown in Fig. 16. On the other hand, an emittance blow-up of a factor about 100 larger than the tolerated one is observed for the pulse $R_{0.5}$, even if the strength of the residual kick is reduced to 1 nrad. The growth is visible only in the vertical plane, as expected, because in these simulations the linear coupling is perfectly corrected (see Table 3). Effects of a realistic value of linear coupling are discussed in Sect. 8.

7.1 Emittance growth mitigation

The pulse $R_{0.5}$ is the most efficient in terms of beam halo depletion. On the other hand, numerical simulations clearly indicate that such a pulse would be unusable with the current HEL design, given the estimated residual kick of 5 nrad, which would lead to an increase in normalised emittance from $2.5 \mu\text{m}$ to $3 \mu\text{m}$ in about 10 s. Thus, several studies were performed to identify possible strategies to mitigate the observed beam-core blow-up.

A possible option would be reducing the probability p , as this can be done without reducing significantly the halo-depletion performance. Parametric studies were carried out, also with the aim to provide input on required magnetic design quality and the maximum acceptable residual kick on the beam core. The estimated emittance growth as a function of residual kick is presented in Fig. 17a, for different values of p . The core blow-up can be reduced by about a factor 2 going from the pulse $R_{0.5}$ to $R_{0.15}$, without losing significant halo-depletion performance as shown in Fig. 18.

A reduction of the electron beam current would be another mitigation measure. However, assuming a linear scaling of the residual kick, considering that 5 nrad is the estimated residual kick for $I_e = 5 \text{ A}$, it is clear that reaching a residual kick of 0.1 nrad, which would lead to an emittance growth still at the edge of the tolerated value, is not feasible.

A transverse active damper (ADT) is present in the LHC [75] and, although its effect on the beam dynamics is not implemented in SixTrack yet, analytical models can be used to estimate the emittance growth suppression factor [76], which depends only on the tune spread and ADT gain. Thus, considering the nominal ADT damping time of 50 turns [17]

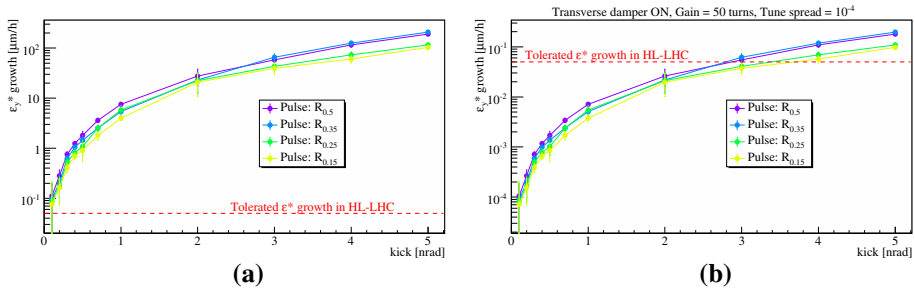


Fig. 17 Emittance growth as a function of residual kick for different values of p for the pulse R_p and $I_e = 5\text{ A}$ without (a) and with (b) the transverse active damper

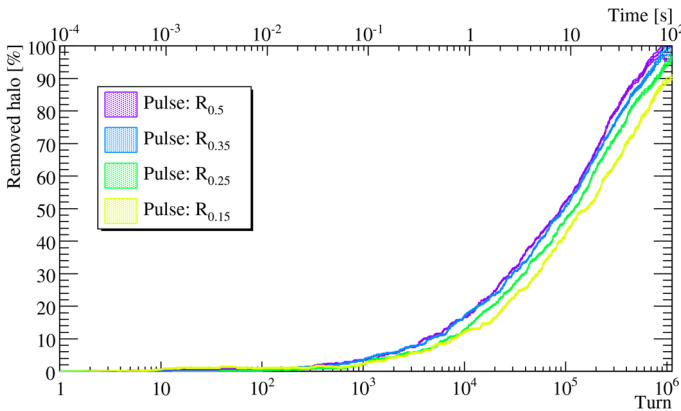


Fig. 18 Halo removed over 100s with a random HEL pulse with different probabilities to switch on the electron beam and $I_e = 5\text{ A}$

and a tune spread of about 10^{-4} with non-colliding beams, a suppression of the emittance growth by a factor about 10^3 is expected, leading to the estimates shown in Fig. 17b. Thus, the pulse $R_{0.25}$ with $I_e = 3\text{ A}$ (i.e. inducing a 3 nrad residual kick) would make the present magnetic design compatible even with a continuous operation of the HEL before bringing the beams in collision. Note that when beams are colliding the tune spread is dominated by head-on beam–beam, which reaches a value of 0.168 from each of the two high-luminosity interaction points [17], hence reducing the emittance growth suppression factor to a value of about 3. Thus, the pulse R_p is not usable for beam halo depletion with colliding beams.

Of course, the ADT acts on particles in both the beam core and tails. However, its impact on the two populations is different, given the intrinsically nonlinear motion of halo particles. Thus, the tails re-population rate will be certainly affected by the ADT, but this should not interfere with the halo removal process controlled by the HEL. A detailed analysis of the interplay between ADT and HEL for the case of halo particles is planned, with the goal to shed some light on the process and to establish quantitative conclusions.

Simulations of beam-core blow-up were also performed for the pulse R_I , showing an emittance growth rate equivalent to the pulse $R_{0.5}$ with $I_e = 3\text{ A}$. This observation, together with equivalent halo-depletion performance (see Fig. 11), supports that the assumption of linear scaling of the residual kick with I_e is reasonable. Nevertheless, a linear assumption is the lowest-order approximation of any more complicated dependence, which should be

assessed by means of dedicated electron beam dynamic simulations. In conclusion, these results show once more that the expected performance of the pulse R_I would not justify the required efforts to make it feasible from the hardware side.

8 Towards scenarios for the operational use of HEL in HL-LHC

Some additional factors must be taken into account to refine the possible operational scenarios that have been sketched for the use of HEL in HL-LHC, which are discussed in the following.

The electron beam must be pulsed to comply with machine-protection constraints introduced in Sect. 2.2, regardless of the operational pattern used. Of course, the electron beam will not be identical from pulse to pulse and the effect of unexpected limited reproducibility must be estimated. A 1% pulse-to-pulse stability was taken considering it as a pessimistic assumption, although such a stability level has to be confirmed at the test stand that is under construction at CERN. A random component with a Gaussian distribution cut at 3σ and $\sigma = 1\%$ was added to either electron beam current or residual kick in the case of beam halo depletion or core blow-up study, respectively. No effects have been observed on emittance growth or on beam halo depletion performance for the pulses $R_{0.5}$, P_9^{14} , DC, except for a minor increase in beam halo depletion with DC pulse, because of the additional random component provided by the pulse-to-pulse variation of the electron beam current.

The effect of linear coupling must also be taken into account for a more realistic evaluation of beam-core blow-up, as the actual system invariant is provided by the sum of the normalised emittances in the two transverse planes. The target coupling correction in HL-LHC is of a few 10^{-3} [17] and a dedicated set of numerical simulations has been performed in which the skew quadrupoles are used to generate linear coupling along the ring in a way in which both amplitude and phase ϕ can be controlled so that their effect can be clearly disentangled. The estimated expected sharing of emittance blow-up between planes is shown in Fig. 19, from which it is visible that:

- The larger the amplitude, the larger the sharing between planes, for $50 < \phi < 320$ deg.
- The larger the amplitude, the smaller the sharing between planes, for $130 < \phi < 230$ deg.
- The larger the amplitude, the larger the sharing between planes, but most of the growth still in the excitation plane, for $50 < \phi < 130$ deg and $230 < \phi < 320$ deg.

Thus, the linear coupling could be used to redistribute possible effects on the core emittance, for instance to avoid luminosity unbalance between the two high-luminosity experiments due to the crossing scheme geometrical factor. It is worth noting, however, this must be combined with other beam stability considerations that rely on linear coupling phase, which would be additional constraints to the management of linear coupling effects.

The transverse tunes of HL-LHC have been carefully optimised to provide the best beam lifetime in the various stages of the operational cycle. This has been accomplished by using the LHC experience gathered during the Run 1 and 2. Two sets of tune values are used for injection and collision conditions, corresponding to (62.27, 60.295) [17] and (62.31, 60.32) (see Table 3), respectively. A key point is to verify the dependence of the HEL performance on the transverse tunes in order to assess whether there is any constraint on the time of the change between them in the operational cycle.

Beam halo-depletion performance obtained with both tune sets for the pulses $R_{0.5}$ and DC are very similar. In particular, more than 45% and less than 1% removed halo after 10 s have been observed for the pulses $R_{0.5}$ and DC, respectively. The main difference is the performance of the pulse P_j^i , as it is expected to be strongly dependent on the tune footprint,

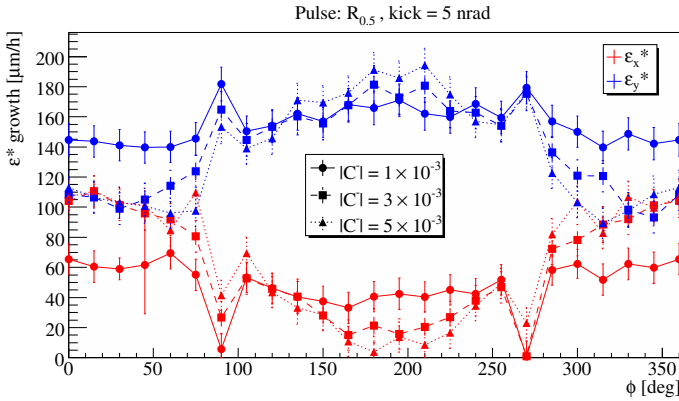


Fig. 19 Emittance growth in the two transverse planes as a function of linear coupling amplitude and phase

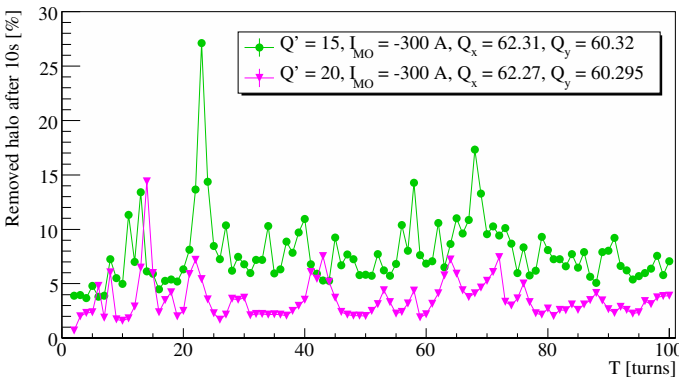


Fig. 20 Estimated beam halo removal after 10 s as a function of pulse period T , for different tune values

as discussed in Sect. 6.2, which in turn depends on the linear tune values. In particular, it has been observed that the most efficient period moved from $T = 23$ turns with collision tunes to $T = 14$ turns with injection tunes, with relative most efficient pulse type changing from P_9^{14} to P_7^7 , although P_7^7 is expected to be less efficient than P_9^{14} , as shown in Fig. 20.

Furthermore, an overall reduction of removed beam halo after 10 s can be seen in Fig. 20 for all pulses, which may be explained by the increased distance to the third-order resonance when using the injection tunes.

Equivalent conclusions can be drawn regarding the effects on the emittance of the beam core. No emittance growth is expected with pulses DC and P_7^7 , while the same blow-up is observed with R_p pulse. Thus, the same mitigation strategy discussed in Sect. 7.1 can be applied.

Combining these results and considerations with what presented in Sects. 6 and 7, a possible strategy for an optimised operational use of HEL in HL-LHC could be:

- Before bringing the beams in collision, the pulse R_p should be used, provided a fine-tuning of I_e , p and the duration of the excitation is performed, depending on the residual kick of the final HEL design that is being optimised. The pulse $R_{0.25}(R_{0.5})$ with 3(2) nrad of residual kick would be compatible with a continuous beam halo depletion. If continuous

depletion is not deemed necessary, 100 s are sufficient for an almost complete beam halo removal and HEL can be triggered when needed.³

- After the beams are brought into collision, the continuous use of the pulse P_9^{14} should be selected, as it provides largest beam halo removal without inducing emittance blow-up.

If the beam-core blow-up induced by the pulse R_p cannot be efficiently mitigated, or the removal rate of P_7^7 would not be sufficient, these studies may suggest performing the tune change from injection to collision values as soon as the beam has reached 7 TeV, to then use the pulse P_9^{14} for continuous halo depletion also before bringing the beams in collision.

9 Conclusions and outlook

Detailed beam dynamics calculations have been presented, showing promising expectations on HEL performance in HL-LHC and providing key inputs towards the finalisation of specifications and operational scenarios.

Studies of DA and FMA have been used to explore the available parameter space and to define a subset of HEL configurations. Following this, a detailed evaluation of halo depletion and effect on the beam core has been performed. In particular, FMA can provide a qualitative overview of the tune footprint distortion caused by the HEL that couples with machine nonlinearities, broadening regions of lower stability. It has been demonstrated that DA simulations can provide a qualitative performance comparison between different HEL pulsing patterns, together with a first quantitative estimation of the time needed to completely deplete the primary beam halo by a given HEL pulse pattern, which is achieved when DA reaches r_1 . Nevertheless, detailed halo-depletion simulations combined with studies on possible detrimental effects on the beam core are needed for a complete and quantitative evaluation of expected HEL performance.

A generalised approach in the definition of deterministic pulsing pattern allowed to identify the innovative and promising pattern P_9^{14} , which could significantly enhance halo removal performance with respect to the DC excitation. Both pulses have been found to induce an emittance growth within the acceptable limit of 0.05 $\mu\text{m}/\text{h}$, making them compatible with a continuous depletion also with the present HEL magnetic design that features a residual kick of about 5 nrad in the vertical plane.

The most efficient pulse in terms of halo depletion is the random excitation R_p , with constant electron beam current. On the other hand, it has been shown that the present residual field induces an unacceptable core blow-up. However, margins on electron beam current and on probability to be switched on have been studied and combined with the effect of the transverse active damper. An optimised HEL magnetic design with a residual kick below 3 nrad would make it possible even to continuously use R_p when the beams are not colliding.

Present studies show that requirements on the availability of pulsing patterns involving variation of electron beam current on a turn-by-turn basis can be relaxed. Equivalent performance can be obtained with pulses that are much easier to achieve from the hardware point of view.

A first proposal of a possible operational scenario in HL-LHC has been presented, which is based on the above considerations combined with additional factors, such as: pulse-to-pulse stability, target coupling correction, dependence on the transverse tunes.

One of the main open points is the detailed understanding of the underlying physics process and its dependencies that lead to the resonant structures visible when using deterministic

³ This mode of operation is similar to the abort gap cleaning.

pulsing patterns. Attempts were made in order to produce a simple analytical model that would allow to predict the optimal pulse without the need of complete tracking simulations. However, work is still ongoing and will be part of a dedicated publication.

Finally, one of the main aims of this paper is to provide an overview of expected beam dynamics with HEL in HL-LHC. However, some key studies will need to be finalised once the operational cycle and optics will be frozen. Of course, there are no significant changes expected because strong nonlinearities are present in the lattice used, which are the main driving term of HEL performance. On the other hand, the tune footprint is significantly affected by head-on beam–beam and it would be certainly interesting to repeat the studies reported here for the pulses DC and P_j^i taking it into account (the pulse R_p cannot be used anyway with colliding beams because of the induced emittance growth).

Acknowledgements The authors greatly acknowledge all BOINC volunteers who supported LHC@Home project, giving for free their CPU time and allowing these results to be produced. One of the authors (D. Mirarchi) warmly thanks X. Buffat, F. Van Der Veken, and S. Kostoglou for their help in analytical evaluation of the transverse damper properties, setting up of dynamic aperture simulations, and setting up of frequency map analysis environment, respectively. The authors are grateful to the members of the HL-LHC Work-Package 2 and 5 for useful inputs and discussions. Last but not least, a personal thank-you goes to Y. Papaphilippou, O. Brüning, G. Arduini, and R. Jones for fruitful comments and suggestions about the original version of this manuscript.

Funding Open access funding provided by CERN (European Organization for Nuclear Research)

Data Availability Statement This manuscript has no associated data or the data will not be deposited. [Authors' comment: All the relevant data are either reported in the paper or can be derived analytically using the formalism described and using open-source software cited.]

Open Access This article is licensed under a Creative Commons Attribution 4.0 International License, which permits use, sharing, adaptation, distribution and reproduction in any medium or format, as long as you give appropriate credit to the original author(s) and the source, provide a link to the Creative Commons licence, and indicate if changes were made. The images or other third party material in this article are included in the article's Creative Commons licence, unless indicated otherwise in a credit line to the material. If material is not included in the article's Creative Commons licence and your intended use is not permitted by statutory regulation or exceeds the permitted use, you will need to obtain permission directly from the copyright holder. To view a copy of this licence, visit <http://creativecommons.org/licenses/by/4.0/>.

References

1. R. Assmann et al., The final collimation system for the LHC. Tech. rep. (2006)
2. R.W. Assmann, Collimators and beam absorbers for cleaning and machine protection, in *Proceedings of the LHC Project Workshop—Chamonix XIV, Chamonix, France* (2005), p. 261
3. R. Bruce et al., Simulations and measurements of beam loss patterns at the CERN Large Hadron Collider. Phys. Rev. Special Top. Accel. Beams **17**(8), 081004 (2014)
4. G. Valentino et al., Final implementation, commissioning, and performance of embedded collimator beam position monitors in the Large Hadron Collider. Phys. Rev. Accel. Beams **20**, 081002 (2017). <https://doi.org/10.1103/PhysRevAccelBeams.20.081002>
5. G. Valentino et al., Semiautomatic beam-based LHC collimator alignment. Phys. Rev. ST Accel. Beams **15**, 051002 (2012). <https://doi.org/10.1103/PhysRevSTAB.15.051002>
6. R. Bruce, R.W. Assmann, S. Redaelli, Calculations of safe collimator settings and β^* at the CERN Large Hadron Collider. Phys. Rev. ST Accel. Beams **18**, 061001 (2015). <https://doi.org/10.1103/PhysRevSTAB.18.061001>
7. R.W. Assmann, in *12th Chamonix LHC Performance Workshop* (2003), pp. 163–170
8. N. Fuster Martinez et al., in *LHC Beam Operations Workshop* (2019)
9. G. Apollinari, High Luminosity Large Hadron Collider HL-LHC. CERN Yellow Rep. **5**, 1 (2016)
10. B. Alonso, L. Rossi, HiLumi LHC Technical Design Report. Tech. rep., CERN-ACC-2015-0140 (2015)

11. HL-LHC Preliminary Design Report: FP7 HiLumi LHC Deliverable D1.5. Tech. rep., CERN-ACC-2014-0300 (2014)
12. G. Arduini et al., High luminosity LHC: challenges and plans. *J. Instrum.* **11**(12), C12081 (2016)
13. O. Brüning, High Luminosity LHC Technical Design Report. Tech. rep, In preparation (2020)
14. G. Valentino et al., Beam diffusion measurements using collimator scans in the LHC. *Phys. Rev. Special Top. Accel. Beams* **16**(2), 021003 (2013)
15. G. Valentino, What did we learn about HALO population during MDs and regular operation? Presented at Review of the needs for a hollow e-lens for the HL-LHC (2016). <https://indico.cern.ch/event/567839/>
16. A. Gorzawski et al., Probing LHC halo dynamics using collimator loss rates at 6.5 Tev. *Phys. Rev. Accel. Beams* **23**(4), 044802 (2020)
17. E. Metral et al., Update of the HL-LHC operational scenarios for proton operation (2018). <https://cds.cern.ch/record/2301292>
18. S. Redaelli et al., Hollow electron lenses for beam collimation at the high-luminosity large hadron collider (HL-LHC). *J. Instrum.* **16**(03), P03042 (2021)
19. A. Santamaría García et al., in *Proceedings of IPAC* (2016), p. TUPMW025
20. K. Sjobak, et al., in *7th International Particle Accelerator Conference* (2016), p. THPOY043. <https://doi.org/10.18429/JACoW-IPAC2016-THPOY043>
21. Review of the needs for a hollow e-lens for the HL-LHC. <https://indico.cern.ch/event/567839/>
22. International review on the e-lens concept readiness for integration into the HL-LHC baseline. <https://indico.cern.ch/event/648237/>
23. International review of the HL-LHC collimation system. <https://indico.cern.ch/event/780182/>
24. V. Shiltsev et al., Experimental demonstration of colliding-beam-lifetime improvement by electron lenses. *Phys. Rev. Lett.* **99**(24), 244801 (2007)
25. X.L. Zhang et al., Generation and diagnostics of uncaptured beam in the Fermilab Tevatron and its control by electron lenses. *Phys. Rev. Special Top. Accel. Beams* **11**(5), 051002 (2008)
26. G. Stancari, A. Valishev, in *ICFA Mini-Workshop on Beam-Beam Effects in Hadron Colliders* (CERN, 2013), pp. 121–125
27. G. Stancari, Characterization of the CERN hollow electron gun at the Fermilab electron-lens test stand? Presented at 84th Collimation upgrade specification meeting (2017). <https://indico.cern.ch/event/623634/>
28. G. Stancari et al., Collimation with hollow electron beams. *Phys. Rev. Lett.* **107**(8), 084802 (2011)
29. G. Stancari, G. Annala, T. Johnson, D. Still, A. Valishev, in *Proceedings of the 11th International Particle Accelerator Conference* (2011), p. 1882
30. X. Gu, M. Okamura, A. Pikin, W. Fischer, Y. Luo, The effects of realistic pancake solenoids on particle transport. *Nucl. Instrum. Methods Phys. Res. Sect. A Accel. Spectrom. Detect. Assoc. Equip.* **637**(1), 190 (2011)
31. Y. Luo et al., Six-dimensional weak-strong simulation of head-on beam–beam compensation in the relativistic heavy ion collider. *Phys. Rev. Special Top. Accel. Beams* **15**(5), 051004 (2012)
32. X. Gu et al., The electron lens test bench for the relativistic heavy ion collider at Brookhaven National Laboratory. *Nucl. Instrum. Methods Phys. Res. Sect. A Accel. Spectrom. Detect. Assoc. Equip.* **743**, 56 (2014)
33. W. Fischer et al., Operational head-on beam–beam compensation with electron lenses in the relativistic heavy ion collider. *Phys. Rev. Lett.* **115**(26), 264801 (2015)
34. Y. Luo, W. Fischer, S. White, Analysis and modeling of proton beam loss and emittance growth in the relativistic heavy ion collider. *Phys. Rev. Accel. Beams* **19**(2), 021001 (2016)
35. P. Thieberger et al., High energy Coulomb-scattered electrons for relativistic particle beam diagnostics. *Phys. Rev. Accel. Beams* **19**(4), 041002 (2016)
36. X. Gu et al., Electron lenses for head-on beam-beam compensation in RHIC. *Phys. Rev. Accel. Beams* **20**(2), 023501 (2017)
37. W. Fischer et al., Compensation of head-on beam–beam induced resonance driving terms and tune spread in the relativistic heavy ion collider. *Phys. Rev. Accel. Beams* **20**(9), 091001 (2017)
38. X. Gu et al., Halo removal experiments with hollow electron lens in the BNL relativistic heavy ion collider. *Phys. Rev. Accel. Beams* **23**(3), 031001 (2020)
39. M. Fitterer, G. Stancari, A. Valishev, S. Redaelli, D. Valuch, Resonant and random excitations on the proton beam in the Large Hadron Collider for active halo control with pulsed hollow electron lenses. *Phys. Rev. Accel. Beams* **24**(2021). <https://doi.org/10.1103/PhysRevAccelBeams.24.021001>
40. S. Redaelli et al., Plans for integration of hollow electron lenses for hadron beam collimation at the HL-LHC. *J. Instrum.* (In preparation) (2021)
41. R. Veness et al., Development of a beam-gas curtain profile monitor for the high luminosity upgrade of the LHC p. WEPB16. 5 p (2019). <https://doi.org/10.18429/JACoW-IBIC2018-WEPB16>

42. H. Zhang et al., A supersonic gas jet-based beam profile monitor using fluorescence for HL-LHC p. WEPAF034, 4 p (2018). <https://doi.org/10.18429/JACoW-IPAC2018-WEPAF034>
43. R. Bruce, Operational aspects and machine protection considerations. Presented at international review on the e-lens concept readiness for integration into the HL-LHC baseline (2017). <https://indico.cern.ch/event/648237/>
44. G. Arduini, Potential performance reach for the HL-LHC in case of a depleted beam halo. Presented at review of the needs for a hollow e-lens for the HL-LHC (2016). <https://indico.cern.ch/event/567839/>
45. E.B. Holzer et al., Beam loss monitoring for LHC machine protection. *Physics Procedia* **37**, 2055 (2012)
46. D. Wollmann, Potential failure scenarios that can lead to very fast orbit changes and machine protection requirements for HL-LHC operation. Presented at review of the needs for a hollow e-lens for the HL-LHC (2016). <https://indico.cern.ch/event/567839/>
47. B. Salvachua, S. Redaelli, Loss and lifetime observations during nominal operation and their extrapolation to HL-LHC parameters. Presented at review of the needs for a hollow e-lens for the HL-LHC (2016). <https://indico.cern.ch/event/567839/> <https://indico.cern.ch/event/567839/>
48. F. Schmidt, SixTrack, User's Reference Manual. Tech. rep., CERN SL/94-56 (AP) (1994)
49. <http://sixtrack.web.cern.ch/SixTrack/>
50. G. Robert-Demolaize, R. Assmann, S. Redaelli, F. Schmidt, in *Proceedings of the Particle Accelerator Conference, 2005. PAC 2005* (IEEE, 2005), pp. 4084–4086
51. <http://lhc-collimation-project.web.cern.ch/lhc-collimation-project/code-tracking-2012.php>
52. CERN, *ICFA Mini-Workshop on Tracking for Collimation in Particle Accelerators: CERN, Geneva, Switzerland 30 Oct 2015. ICFA Mini-Workshop on Tracking for Collimation in Particle Accelerators* (CERN, Geneva, 2018). <https://doi.org/10.23732/CYRCP-2018-002>
53. P. Hermes et al., Measured and simulated heavy-ion beam loss patterns at the CERN Large Hadron Collider. *Nucl. Instrum. Methods Phys. Res. Sect. A Accel. Spectrom. Detect. Assoc. Equip.* **819**, 73 (2016)
54. R. Bruce et al., Reaching record-low β^* at the CERN Large Hadron Collider using a novel scheme of collimator settings and optics. *Nucl. Instrum. Methods Phys. Res. Sect. A Accel. Spectrom. Detect. Assoc. Equip.* **848**, 19 (2017)
55. R. Bruce et al., Collimation-induced experimental background studies at the CERN large hadron collider. *Phys. Rev. Accel. Beams* **22**(2), 021004 (2019)
56. A. Gorzawski et al., Collimation of partially stripped ions in the CERN large hadron collider. *Phys. Rev. Accel. Beams* **23**, 101002 (2020). <https://doi.org/10.1103/PhysRevAccelBeams.23.101002>
57. D. Mirarchi et al., Reducing beam-related background on forward physics detectors using crystal collimation at the large hadron collider. *Phys. Rev. Appl.* **14**, 064066 (2020). <https://doi.org/10.1103/PhysRevApplied.14.064066>
58. N. Fuster-Martínez et al., Simulations of heavy-ion halo collimation at the CERN large hadron collider: benchmark with measurements and cleaning performance evaluation. *Phys. Rev. Accel. Beams* **23**, 111002 (2020). <https://doi.org/10.1103/PhysRevAccelBeams.23.111002>
59. <https://boinc.berkeley.edu/>
60. <https://lhathome.web.cern.ch/home>
61. <https://lhathome.web.cern.ch/projects/sixtrack>
62. G. Stancari, Calculation of the transverse kicks generated by the bends of a hollow electron lens (2014)
63. J. Laskar, *Introduction to Frequency Map Analysis* (Springer, Dordrecht, 1999), pp. 134–150
64. R. Bartolini, A. Faus-Golfe, M. Giovannozzi, E. Todesco, W. Scandale, Early indicators of long term stability in hadron colliders (LHC-Project-Report-41. CERN-LHC-Project-Report-41) (1996)
65. M. Giovannozzi, W. Scandale, E. Todesco, Prediction of long-term stability in large hadron colliders. *Part. Accel.* **56**, 195 (1996)
66. V.D. Shiltsev, *Electron Lenses for Super-Colliders*. Particle Acceleration and Detection (Springer, Berlin, 2016). <https://doi.org/10.1007/978-1-4939-3317-4>
67. E. Todesco, M. Giovannozzi, Dynamic aperture estimates and phase-space distortions in nonlinear betatron motion. *Phys. Rev. E* **53**, 4067 (1996). <https://doi.org/10.1103/PhysRevE.53.4067>
68. M. Giovannozzi, W. Scandale, E. Todesco, Dynamic aperture extrapolation in presence of tune modulation. *Phys. Rev. E* **57**, 3432 (1998). <https://doi.org/10.1103/PhysRevE.57.3432>
69. A. Bazzani et al., Advances on the modeling of the time evolution of dynamic aperture of hadron circular accelerators. *Phys. Rev. Accel. Beams* **22**, 104003 (2019). <https://doi.org/10.1103/PhysRevAccelBeams.22.104003>
70. M. Giovannozzi, A proposed scaling law for intensity evolution in hadron storage rings based on dynamic aperture variation with time. *Phys. Rev. ST Accel. Beams* **15**, 024001 (2012). <https://doi.org/10.1103/PhysRevSTAB.15.024001>

71. M. Giovannozzi, F.F. Van der Veken, Description of the luminosity evolution for the CERN LHC including dynamic aperture effects. Part I: the model. Nucl. Instrum. Methods Phys. Res. **A905**, 171 (2018). <https://doi.org/10.1016/j.nima.2019.01.072>
72. M. Giovannozzi, F.F. Van der Veken, Description of the luminosity evolution for the CERN LHC including dynamic aperture effects. Part II: application to Run 1 data. Nucl. Instrum. Methods Phys. Res. **A908**, 1 (2018). <https://doi.org/10.1016/j.nima.2018.08.019>
73. A. Bazzani et al., Advances on the modeling of the time evolution of dynamic aperture of hadron circular accelerators. Phys. Rev. Accel. Beams **22**(10), 104003 (2019)
74. A. Mereghetti, Status of simulations and required inputs. Presented at 122nd collimation upgrade specification meeting (2019). <https://indico.cern.ch/event/865924/>
75. P. Baudrenghien et al., LHC Transverse feedback system and its hardware commissioning (LHC-PROJECT-Report-1148. CERN-LHC-PROJECT-Report-1148), 4 p (2008). <https://cds.cern.ch/record/1124090>
76. X. Buffat, W. Herr, T. Pieloni, D. Valuch, Modeling of the emittance growth due to decoherence in collision at the large hadron collider. Phys. Rev. Accel. Beams **23**(2), 021002 (2020)